

ZnSnS₃: Structure Prediction, Ferroelectricity, and Solar Cell Applications

Radi A. Jishi*

Department of Physics, California State University, Los Angeles, California, U.S.A

Marcus A. Lucas†

Department of Electrical Engineering, California State University, Los Angeles, California, U.S.A

(Dated: June 13, 2016)

The rapid growth of the solar energy industry has produced a strong demand for high performance, efficient photoelectric materials. Many ferroelectrics, composed of earth-abundant elements, are useful for solar cell applications due to their large internal polarization. However, their wide band gaps prevent them from absorbing light in the visible to mid-infrared range. Here, we address the band gap issue by investigating, in particular, the substitution of sulphur for oxygen in the perovskite structure ZnSnO₃. Using evolutionary methods we identify the stable and metastable structures of ZnSnS₃ and compare them to those previously characterized for ZnSnO₃. Our results suggest that ZnSnS₃ forms a monoclinic structure followed by metastable ilmenite and lithium-niobate structures. The latter structure is highly polarized and it possesses a significantly reduced band gap of 1.28 eV. These desirable characteristics make it a prime candidate for solar cell applications.

Keywords: Structure prediction, evolutionary methods, ZnSnO₃, ZnSnS₃, ferroelectrics, mBJ, solar cells,

I. INTRODUCTION

Ferroelectrics are materials that possess spontaneous electric polarization. This results from a lack of inversion symmetry; all ferroelectric crystals are non-centrosymmetric. Due

*Electronic address: rjishi@calstatela.edu

†Electronic address: mlucas9@calstatela.edu

to intrinsic polarization, ferroelectrics may serve as light harvesters in photovoltaic devices [1–6]. In a semiconductor p-n junction acting as a photovoltaic device, the built-in potential across the depletion layer is used to separate the photoexcited electron-hole pairs; the maximum open-circuit voltage is thus almost equal to the semiconductor band gap. In a ferroelectric, on the other hand, the separation of the photoexcited pairs is due to the built-in potential induced by the intrinsic polarization; this makes possible the realization of open-circuit voltages that far exceed the band gap [7–17].

Among the most important ferroelectrics are metal oxide perovskites with the general formula ABO_3 , where A and B are metal cations (usually, B is a transition metal). Well-known examples of such ferroelectrics are $BaTiO_3$ and $LiNbO_3$. These oxides have relatively large internal electric fields that could be exploited in photovoltaic applications. However, progress in this area has been hampered by the fact that these ferroelectrics have a large band gap (3-4 eV), which makes them unsuitable to function as efficient light harvesters. The large band gap is due to the strong ionic bonding between the transition metal B and oxygen, which, in turn, is due to the large difference in electronegativity between these atoms. In ABO_3 , the highest valence band is derived from oxygen 2p orbitals, while the low conduction bands are derived from the transition metal 3d states.

To reduce the band gap in ferroelectrics, different strategies have been implemented. Choi et al. [18] alloyed the ferroelectric $Bi_4Ti_3O_{12}$, which has an optical band gap between 3.1 and 3.6 eV [19–21], with $LaCoO_3$, which is a Mott insulator with a small band gap of 0.1 eV [22]. From X-ray diffraction and scanning transmission electron microscopy they concluded that some La atoms substitute for some Bi atoms at some specific sites, and some Co atoms occupy some Ti sites. Since Co is more electronegative than Ti (1.88 vs 1.54), Co-O bond is less ionic than Ti-O bond, and a reduction in the band gap is expected. Indeed, a reduction of up to 1 eV was observed.

In another approach, Grinberg et al. [23] placed two different transition metal cations on the perovskite B-site, with one atom driving ferroelectricity and the other producing a band gap in the visible range. They mixed the ferroelectric oxide potassium niobate ($KNbO_3$) with barium nickel niobate ($BaNi_{1/2}Nb_{1/2}O_{3-\delta}$) so as to introduce Ni^{2+} on the B-site along with an oxygen vacancy which can give rise to gap states in the host $KNbO_3$ crystal. The solid solutions thus formed, $[KNbO_3]_{1-x}[BaNi_{1/2}Nb_{1/2}O_{3-\delta}]_x$ with $x = 0.1$ to 0.5, were ferroelectric with a direct band gap ranging from 1.1-3.38 eV.

In some multiferroics, which exhibit a magnetic order along side the ferroelectric one, a somewhat smaller band gap exists. In BiFeO_3 the band gap is 2.7 eV [24, 25]. It is thus expected that multiferroics, such as BiFeO_3 and $\text{Bi}_2\text{FeCrO}_6$ [26, 27], would be more promising candidates for solar cell applications. In $\text{Bi}_2\text{FeCrO}_6$ epitaxial thin films, the optical band gap depends on the degree of Fe-Cr ordering. This dependence results from the hybridization of the 3d orbitals in Fe and Cr with the 2p orbitals in oxygen. Nechache et al. [28] investigated the effect on the band gap of Fe/Cr ordering and found that, under the right film growth conditions, the band gap can be tuned all the way from 2.7 eV down to 1.5 eV.

An important class of ferroelectric oxides are those that crystallize in the LiNbO_3 structure (LN-structure) with space group $R3c$. These crystals are non-centrosymmetric with a large polarization. LN- ZnSnO_3 , synthesized under a pressure of 7 GPa [29], has a polarization given by $59 \mu\text{C}/\text{cm}^2$. Other LN-type polar oxides synthesized under high pressure include CdPbO_3 [30], PbNiO_3 [30, 31], GaFeO_3 [32], and LiOsO_3 [33]. Ilmenite ZnGeO_3 transforms to an orthorhombic perovskite phase at 30 GPa, and upon releasing the pressure, to the LN-structure [34, 35] with a polarization of about $60 \mu\text{C}/\text{cm}^2$ [36, 37]. Several other LN-type oxides, such as MnTiO_3 [38–41], MnSnO_3 [42, 43], FeTiO_3 [39, 43–45], FeGeO_3 [46], MgGeO_3 [35, 39, 47], and CuTaO_3 [48] were similarly obtained during decompression from the perovskite-type phase, which is stable at high pressure. More recently, LN-type ZnTiO_3 , with a large polarization of $88 \mu\text{C}/\text{cm}^2$, has been synthesized in this fashion [49].

Polar oxide semiconductors of the LN-type have wide band gaps. For example, ZnSnO_3 has a band gap of 3.3-3.7 eV [50, 51]; such values are typical for this class of materials. However, it has been noted that the band gap in ZnSnO_3 is very sensitive to variations in the lattice constants, and suggestions have been made to tune the band gap by growing ZnSnO_3 films on a substrate with some degree of lattice mismatch [52], by substituting sulfur for oxygen [53], or by substitutional doping with calcium or barium [54].

In this work, we carry out first-principles calculations, using density functional theory (DFT), on three LN-type crystals with large remnant polarization, namely, ZnSnO_3 , ZnGeO_3 , and ZnTiO_3 . We show that, upon using the modified Becke-Johnson (mBJ) exchange potential [55], the correct sizes of the band gaps are calculated for these crystals. Having established the validity of this computational method in producing the correct band gaps for this family of compounds, we then focus on ZnSnO_3 and study the effect of substitut-

ing sulfur for oxygen. Since the structure of the resulting compound, ZnSnS_3 , is unknown, we carry out extensive calculations using evolutionary algorithms in order to determine its structure. We find that the most stable structure has a monoclinic unit cell, followed by two metastable structures, namely an ilmenite and a lithium niobate (LN) structure. The monoclinic and ilmenite phases are not polar, but the LN-phase is ferroelectric with a large polarization and a small band gap of 1.28 eV.

II. METHODS

To predict the stable and metastable structures of ZnSnS_3 , two different evolutionary methods, implemented in the codes USPEX and CALYPSO, were employed. The USPEX (Universal Structure Predictor: Evolutionary Xtallography) code [56–58], developed by Oganov, Glass, Lyakhov and Zhu, features local optimization, real-space representation and variation operators that mimic natural evolution. The CALYPSO (Crystal structure AnaLYsis by Particle Swarm Optimization) code [59], developed by Wang, Lv, Zhu and Ma, uses local structural optimization and the particle swarm optimization (PSO) method to update structures.

The first step, in both methods, is to generate a population of random crystal structures, each with a symmetry described by a randomly chosen space group. Once a space group is selected, appropriate lattice vectors and atomic positions are generated. Each generated structure is optimized using density functional theory and its free energy (known as the fitness function) is calculated. The structure optimization is carried out using the code VASP [60–62], which uses a plane wave basis for expanding the electronic wave function. Each structure is optimized in four steps, beginning with a coarse optimization and gradually increasing the accuracy. In the last optimization step, the kinetic energy cutoff for plane wave expansion of the wave function is 600 eV. The optimized structures of the initially generated population constitute the first generation, each member being called an individual. A new generation is then produced where some of its members are generated randomly while others are obtained from the best structures (those with lowest energy) of the previous generation. In USPEX, new individuals (offspring) are produced from parent structures by applying variation operators such as heredity, mutation, or permutation. In the PSO method, a new structure is generated from a previous one by updating the atomic positions using an

evolutionary algorithm. The structures in the new generation are optimized, and the best among them serve as precursors for structures in the next generation. The process continues until convergence to the best structures is achieved.

Band gaps, band structures, and densities of states were calculated using the all-electron, full-potential, linearized, augmented plane wave method as implemented in the WIEN2K code [63]. Here, space is divided into two regions. One region comprises the interior of nonoverlapping muffin-tin spheres centered on the atomic sites, while the rest of the space (the interstitial) makes the other region. The electronic wave function is expanded in terms of a set of basis functions which take different forms in the two distinct regions of space. Inside the spheres, the basis functions are atomic-like functions written as an expansion in spherical harmonics up to $l_{max} = 10$. In the interstitial, they are plane waves with a maximum wave vector of magnitude K_{max} . Each plane wave is augmented by one atomic-like function in each muffin-tin sphere. K_{max} was chosen so that $R_{mt}K_{max} = 8$, where R_{mt} is the radius of the smallest muffin-tin sphere in the unit cell. Charge density was Fourier-expanded up to a maximum wave vector of $14 a_0^{-1}$, where a_0 is the Bohr radius. Modified Becke-Johnson exchange potential [55], which is known to yield reasonably accurate band gap values in semiconductors, was adopted in our band structure calculations. In the self-consistent field calculations, the total energy and charge were converged to within 0.1 mRy and 0.001 e, respectively. For total energy calculations, a Monkhorst-Pack [64] 8x8x8 grid of \mathbf{k} -points in the Brillouin zone is used.

III. RESULTS AND DISCUSSION

As a rough guide to predicting the stable structure of a compound of the form ABX_3 , where A and B are cations and X is an anion, one usually calculates the Goldschmidt tolerance factor given by

$$t = \frac{r_A + r_X}{\sqrt{2}(r_B + r_X)} \quad (1)$$

where r_A , r_B , and r_X are the radii of the A, B, and X ions, respectively. For Zn, Sn, O, and S, the ionic radii are given, respectively, by 0.74 Å, 0.69 Å, 1.4 Å, and 1.84 Å. Using these values, we find that for $ZnSnO_3$, $t = 0.724$, while for $ZnSnS_3$, $t = 0.721$. We are thus tempted to conclude that the replacement of oxygen with sulfur should not cause

a change in structure. As stated in the introduction, the most stable phase of ZnSnO_3 is the ilmenite structure (space group R-3) which, upon application and subsequent release of pressure, transforms to the ferroelectric lithium niobate (LN) phase (space group R3c). One would expect ZnSnS_3 to behave in a similar way. However, the large polarizability of sulfur indicates that the Goldschmidt tolerance factor may not be sufficient for predicting the structure of sulfur-containing compounds [65].

To resolve this issue, we carried out extensive calculations using the evolutionary algorithm implemented in USPEX and the PSO method used by CALYPSO. During the USPEX calculation, 20 generations were produced with each generation containing 20 individuals. In the PSO method we produced 20 generations, each generation consisting of 50 individuals. For all generated structures, the unit cell was assumed to contain two formula units. The most stable structures were identified, each with a specific space group. To analyze the results further, 80 random structures were subsequently generated for each of the most stable space groups. Out of each set of 80 optimized structures, the single structure with the lowest energy was identified. In this fashion, the best structures of ZnSnS_3 , along with their specific space groups, were determined.

In Table 1 we list these ZnSnS_3 structures by order of their stability. To compare the relative stability of various structures, the free energy per atom in the most stable structure is set equal to zero. That structure has a monoclinic unit cell with space group $P2_1$ (number 4). The metastable structure with lowest energy is the ilmenite, followed by the LN-type structure. This is to be contrasted with ZnSnO_3 , where the ilmenite structure is most stable and the LN-phase is a metastable one. Similar to the case of ZnSnO_3 , we expect that ZnSnS_3 would undergo a phase transition from the most stable monoclinic phase to the metastable phase of ilmenite or LN-type under appropriate conditions of temperature and pressure.

To evaluate the relevance of ZnSnS_3 to solar cell applications, we have calculated the band structures of the three most stable phases of this compound. Since low band gap values for the light absorbers are essential for photovoltaic applications, it is important that the computational method yield accurate values for these gaps. Density functional theory, when using the local density approximation (LDA) or generalized gradient approximation (GGA) to approximate the exchange-correlation term, is known to severely underestimate band gaps in semiconductors. The use of the modified Becke-Johnson (mBJ) exchange potential results in a great improvement in the band gap values comparable to that achieved by the

TABLE I: The predicted most stable structures of ZnSnS_3 at atmospheric pressure. The space groups that describe the symmetry of the structures, the lattice constants (in Å), the angles between the lattice vectors (in degrees), and the relative energies per atom (in eV) are shown. For ease of comparison, the energy per atom of the most stable structure is set equal to zero.

Space group (number)	Lattice constants (Å) and angles (degrees)	Energy/atom (eV)
P2 ₁ (4)	a=8.714, b=6.398, c=3.752, $\alpha = \beta = 90, \gamma = 92.362$	0.000
R-3 (148)	a=b=c=7.016, $\alpha = \beta = \gamma = 53.689$	0.040
R3c (161)	a=b=c=6.761, $\alpha = \beta = \gamma = 55.799$	0.068
P6 ₃ /m (176)	a=b=3.737, c=17.405, $\alpha = \beta = 90, \gamma = 120$	0.074
R32 (155)	a=b=c=6.828, $\alpha = \beta = \gamma = 55.122$	0.089
P6 ₃ (173)	a=b=6.187, c=6.431, $\alpha = \beta = 90, \gamma = 120$	0.100
Cc (9)	a=b=6.393, c=10.796, $\alpha = \beta = 88.229, \gamma = 146.963$	0.145
P6 ₃ mc (186)	a=b=3.766, c=16.559, $\alpha = \beta = 90, \gamma = 120$	0.154
R-3c (167)	a=b=c=6.794, $\alpha = \beta = \gamma = 56.359$	0.155

much more expensive GW approximation. For example, consider the case of ZnSnO_3 . It has a measured band gap E_g in the range 3.3-3.7 eV [50, 51]. Our calculations, using GGA, give a band gap of 1.5 eV. On the other hand, using the mBJ exchange potential, we calculate a band gap of 3.4 eV, which is in excellent agreement with experiment. We also calculated the band gaps in ZnGeO_3 and ZnTiO_3 using this same method, and found them to be 3.57 eV and 3.51 eV, respectively. Though experimental values are not available for the band gaps of these two compounds, the calculated values are typical of those encountered in ferroelectric oxides.

In Fig. 1 we present the calculated energy bands and density of states of the monoclinic phase of ZnSnS_3 , with space group P2₁, using the mBJ exchange potential. The band gap is 1.90 eV. Similar calculations on the ilmenite phase of ZnSnS_3 , with the space group R-3, feature a band gap of 2.30 eV. These two phases of ZnSnS_3 are not very useful as light harvesters in solar cells for two reasons: (1) they do not have small band gaps, and (2) they are not polar.

The situation is markedly different for the LN-phase of ZnSnS_3 with space group R3c (number 161). This phase has a low band gap and a large polarization. In Fig. 2 we show

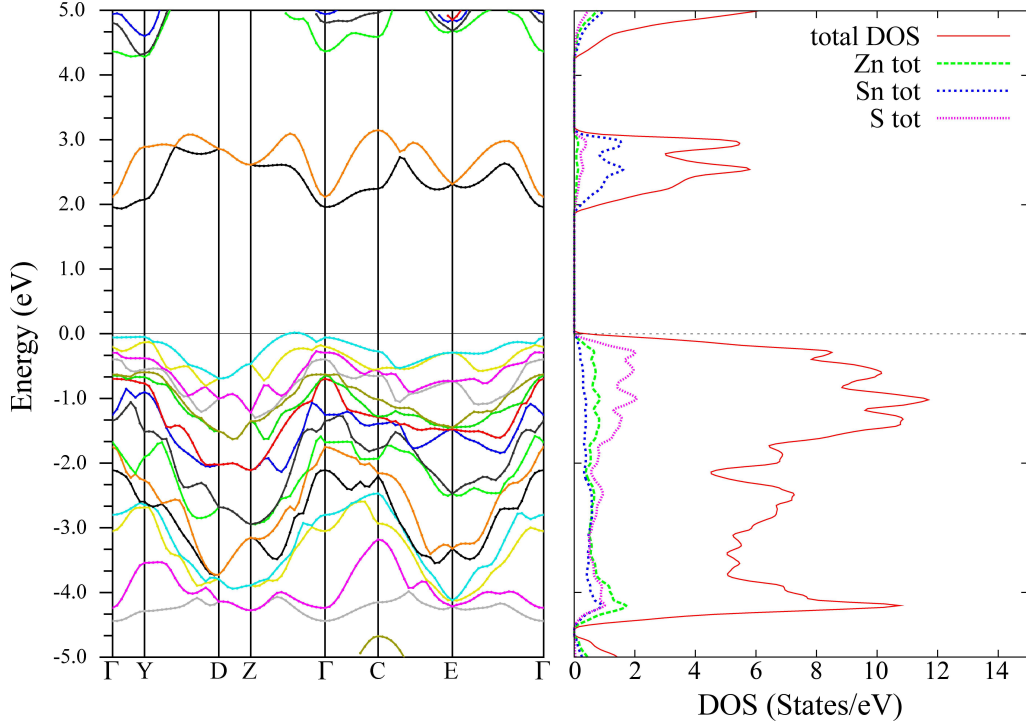


FIG. 1: Energy bands in the monoclinic phase (space group number 4) of ZnSnS_3 , plotted along high symmetry directions, along with a plot of the density of states. The bands are calculated by using the mBJ potential for exchange and correlation. The zero of energy is taken to coincide with the valence band maximum.

the calculated band structure, using the mBJ potential, along with the density of states. Here the band gap is 1.28 eV, in agreement with a previous calculation [53] that used the GW approximation. The upper valence bands are derived mainly from S p-orbitals while the lower conduction bands result mainly from Sn s- and S p-orbitals. The polarization, calculated using the Berry phase formalism of the modern theory of crystal polarization [66, 67], is found to be $57 \mu\text{C}/\text{cm}^2$, which is essentially the same as in the ferroelectric ZnSnO_3 . About one third of the polarization is electronic and the rest is ionic. The large ionic polarization derives from the particular crystal structure of this phase of ZnSnS_3 . Though the Sn ion is octahedrally bonded to six S ions, it does not sit at the center of the octahedron; rather, three of the six Sn-S bonds have a length of 2.42 Å while the other three have a length of 2.57 Å. Hybridization between the Sn s- and S p-orbitals causes a displacement of the Sn ion from the center of the octahedron, thereby lowering the energy of the system.

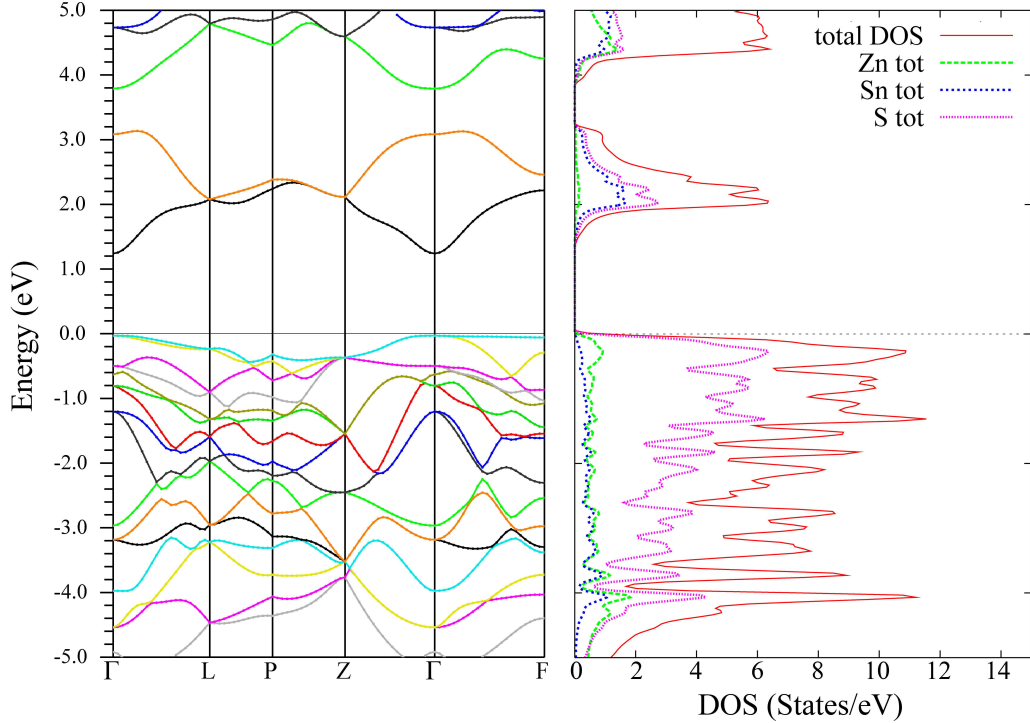


FIG. 2: Energy bands in the LN-phase (space group number 161) of ZnSnS_3 , plotted along high symmetry directions, along with a plot of the density of states. The bands are calculated by using the mBJ potential for exchange and correlation. The zero of energy is taken to coincide with the valence band maximum.

IV. CONCLUSIONS

As anticipated, our calculations indicate that the substitution of sulfur for oxygen in ZnSnO_3 would reduce its band gap, particularly for the LN-phase. This reduction is sufficient to bring the absorption band of ZnSnS_3 into the visible to mid-infrared spectrum, thereby making it a suitable material for solar cell applications. An unexpected result of the substitution is that a monoclinic phase becomes the most stable structure of ZnSnS_3 . However, we assume that, as with ZnSnO_3 , a suitable application of temperature and pressure may be used to transition ZnSnS_3 to its LN-phase. More work must be done to characterize the nature of this transition. The introduction of a stable monoclinic phase in ZnSnS_3 implies that one cannot simply assume that materials generated by substituting another element for oxygen in perovskite oxides will maintain the same relationships between phases. Future analysis should more thoroughly investigate the phases of ZnSnS_3 , evaluating their

stability at a variety of pressures. The transition pathway between phases should also be identified. Finally, the effect of the sulfur for oxygen substitution on other oxides such as ZnGeO_3 and ZnTiO_3 should be considered.

Acknowledgments

The authors gratefully acknowledge support by National Science Foundation under grant No. HRD-0932421 and NSF PREM Program: Cal State L.A. & Penn State Partnership for Materials Research and Education, award DMR-1523588. We also acknowledge partial support by the Materials Simulation Center, at Penn-State and MRI facility.

Conflict of interest

The authors report no conflict of interest in this research.

References

- [1] D. Cao et al., “High-efficiency ferroelectric-film solar cells with an n-type Cu_2O cathode buffer layer,” *Nano Lett.*, vol. 12, no. 6, pp. 2803–2809, 2012.
- [2] M. Alexe and D. Hesse, “Tip-enhanced photovoltaic effects in bismuth ferrite,” *Nature Commun.*, vol. 2, no. 1, Article ID 256, 2011.
- [3] M. Qin, K. Ao, and Y.C. Liang, “High efficiency photovoltaics in nanoscaled ferroelectric thin films,” *Appl. Phys. Lett.*, vol. 93, no. 12, Article ID 122904, 2008.
- [4] T. Choi, S. Lee, Y. Choi, V. Kiryukhlin, and S.-W. Cheong, “Switchable ferroelectric diode and photovoltaic effect in BiFeO_3 ,” *Science*, vol. 324, no. 5923, pp. 63–66 (2009).
- [5] K.T. Butler, J.M. Frost, and A. Walsh, “Ferroelectric materials for solar energy conversion: photoferroics revisited,” *Energy Environ. Sci.*, vol. 8, no. 3, pp. 838–848, 2015.
- [6] Y. Yuan, Z. Xiao, B. Yang, and J. Huang, “Arising applications of ferroelectric materials in photovoltaic devices,” *J. Mater. Chem. A*, vol. 2, no. 17, pp. 6027–6041, 2014.
- [7] S.Y. Yang et al., “Above-bandgap voltages from ferroelectric photovoltaic devices,” *Nature Nanotechnol.*, vol. 5, no. 2, pp. 143–147, 2010.

- [8] Y. Inoue, K. Sato, and H. Miyama, "Photoassisted water decomposition by ferroelectric lead zirconate titanate ceramics with anomalous photovoltaic effects," *J. Phys. Chem.*, vol. 90, no. 13, pp. 2809–2810, 1986.
- [9] S.M. Young and A.M. Rappe, "First-principles calculation of the shift current photovoltaic effect in ferroelectrics," *Phys. Rev. Lett.*, vol. 109, no. 11, Article ID 116601, 2012.
- [10] H. Huang, "Solar energy: Ferroelectric photovoltaics," *Nature Photonics*, vol. 4, no. 3, pp. 134–135, 2010.
- [11] Y. Yuan et al., "Efficiency enhancement in organic solar cells with ferroelectric polymers," *Nature Mater.*, vol. 10, no. 4, pp. 296–302, 2011.
- [12] J.W. Bennett, I. Grinberg, and A.M. Rappe, "New highly polar semiconductor ferroelectrics through d^3 cation-O vacancy substitution in $PbTiO_3$: A theoretical study," *J. Am. Chem. Soc.*, vol. 130, no. 51, pp. 17409–17412, 2008.
- [13] V.M. Fridkin and B. Popov, "Anomalous photovoltaic effect in ferroelectrics," *Sov. Phys. Usp.*, vol. 21, no. 12, pp. 981–991, 1978.
- [14] V.M. Fridkin, Book: "Photoferroelectrics," *Springer*, 1979.
- [15] A. Glass, D. Von der Linde, and T. Negran, "High-voltage bulk photovoltaic effect and the photoreactive process in $LiNbO_3$," *Appl. Phys. Lett.*, vol. 25, no. 4, pp. 233–235, 1974.
- [16] A.G. Chynoweth, "Surface space-charge layers in barium titanate," *Phys. Rev.*, vol. 102, pp. 705–714, 1956.
- [17] G.F. Neumark, "Theory of the Anomalous photovoltaic effect of ZnS ," *Phys. Rev.*, vol. 125, pp. 838–845, 1962.
- [18] W.S. Choi, M.F. Chisholm, D.J. Singh, T. Choi, G.E. Jellison, and H.N. Lee, "Wide band gap tunability in complex transition metal oxides by site-specific substitution," *Nature Commun.*, vol. 3, Article number 689, 2012.
- [19] S. Ehara et al., "Dielectric properties of $Bi_4Ti_3O_{12}$ below the Curie temperature," *Jpn. J. Appl. Phys.*, vol. 20, no. 5, pp. 877–881, 1981.
- [20] D.J. Singh, S.S.A. Seo, and H.N. Lee, "Optical properties of ferroelectric $Bi_4Ti_3O_{12}$," *Phys. Rev. B*, vol. 82, Article ID 180103, 2010.
- [21] C. Jia, Y. Chen, and W.F. Zhang, "Optical properties of aluminum-, gallium-, and indium-doped $Bi_4Ti_3O_{12}$ thin films," *J. Appl. Phys.*, vol. 105, Article ID 113108, 2009.
- [22] T. Arima, Y. Tokura, and J.B. Torrance, "Variation of optical gaps in perovskite-type 3d

- transition-metal oxides,” *Phys. Rev. B*, vol. 48, Article ID 17006, 1993.
- [23] I. Grinberg et al., “Perovskite oxides for visible-light-absorbing ferroelectric and photovoltaic materials,” *Nature*, vol. 503, pp. 509–512, 2013.
 - [24] S.R. Basu, “Photoconductivity in BiFeO₃ thin films,” *Appl. Phys. Lett.*, vol. 92, Article ID 091905, 2008.
 - [25] A.J. Hauser et al., “Characterization of electronic structure and defect states of thin epitaxial BiFeO₃ films by UV-visible absorption and cathodoluminescence spectroscopies,” *Appl. Phys. Lett.*, vol. 92, Article ID 222901, 2008.
 - [26] R. Nechache et al., “Growth, structure and properties of epitaxial thin films of first principles predicted multiferroic Bi₂FeCrO₆,” *Appl. Phys. Lett.*, vol. 89, Article ID 102902, 2006.
 - [27] R. Nechache, C. Harnagea, A. Pignolet, L.-P. Carignan, and D. Ménard, “Epitaxial Bi₂FeCrO₆ multiferroic thin films,” *Phil. Mag. Lett.*, vol. 87, no. 3–4, pp. 231–240, 2007.
 - [28] R. Nechache, C. Harnagea, S. Li, L. Cardenas, W. Huang, J. Chakrabartty, and F. Rosei, “Bandgap tuning of multiferroic oxide solar cells,” *Nature Photonics*, vol. 9, pp. 61–67, 2015.
 - [29] Y. Inaguma, Y. Masashi, and T. Katsumata, “A polar oxide ZnSnO₃ with LiNbO₃ structure,” *J. Am. Chem. Soc.*, vol. 130, no. 21, pp. 6704–6705, 2008.
 - [30] Y. Inaguma, M. Yoshida, T. Tsuchiya, A. Aimi, K. Tanaka, T. Katsumata, and D. Mori, “High-pressure synthesis of novel lithium niobate-type oxides,” *J. Phys.: Conf. Ser.*, vol. 215, no. 1, Article ID 012131, 2010.
 - [31] Y. Inaguma, K. Tanaka, T. Tsuchiya, D. Mori, T. Katsumata, T. Ohba, K. Hiraki, T. Takahashi, and H. Saitoh, “Synthesis, structural transformation, thermal stability, valence state, and magnetic and electronic properties of PbNiO₃ with perovskite and LiNbO₃-type structures,” *J. Am. Chem. Soc.*, vol. 133, no. 42, pp. 16920–16929, 2011.
 - [32] R. Arielly, W.M. Xu, E. Greenberg, G.K. Rozenberg, M.P. Pasternak, G. Garbarino, S. Clark, and R. Jeanloz, “Intriguing sequence of GaFeO₃ structures and electronic states to 70 GPa,” *Phys. Rev. B*, vol. 84, Article ID 094109, 2011.
 - [33] Y. Shi, Y. Guo, X. Wang, A.J. Princep, D. Khalyavin, P. Manuel, Y. Michiue, A. Sato, K. Tsuda, S. Yu, M. Arai, Y. Shirako, M. Akaogi, N. Wang, K. Yamamura, and A.T. Boothroyd, “A ferroelectric-like transition in a metal,” *Nature Mater.*, vol. 12, pp. 1024–1027, 2013.
 - [34] H. Yusa, M. Akaogi, N. Sata, H. Kojitani, R. Yamamoto, and Y. Obishi, “High-pressure trans-

- formations of ilmenite to perovskite, and lithium niobate to perovskite in zinc germanate,” *Phys. Chem. Minerals*, vol. 33, no.3, pp. 217–226, 2006.
- [35] M. Akaogi, H. Kojitani, H. Yusa, R. Yamamoto, M. Kido, and K. Koyama, “High-pressure transitions and thermochemistry of MGeO_3 ($\text{M} = \text{Mg}$, Zn , and Sr) and [50, 51] Sr-silicates: systematics in enthalpies of formation of $\text{A}^{2+}\text{B}^{4+}\text{O}_3$ perovskites,” *Phys. Chem. Minerals*, vol. 32, no. 8, pp. 603–613, 2005.
- [36] J. Zhang, B. Xu, Z. Qin, X.F. Li, and K.L. Yao, “Ferroelectric and nonlinear optical properties of the LiNbO_3 -type ZnGeO_3 from first-principles study,” *J. Alloys and Compounds*, vol. 514, pp. 113–119, 2012.
- [37] Y. Inaguma, A. Aimi, Y. Shirako, D. Sakurai, D. Mori. H. Kojitani, M. Akaogi, and M. Nakayama, “High-pressure synthesis, crystal structure, and phase stability relations of a LiNbO_3 -type polar titanate ZnTiO_3 and its reinforced polarity by the second-order Jahn-Teller effect,” *J. Am. Chem. Soc.*, vol. 136, no. 7, pp. 2748–2756, 2014.
- [38] Y. Syono, S.-L. Akimoto, Y. Ishikawa, and Y. Endoh, “A new high pressure phase of MnTiO_3 and its magnetic property,” *J. Phys. Chem. Solids*, vol. 30, no. 7, pp. 1665–1672, 1969.
- [39] E. Ito and Y. Matsui, “High-pressure transformations in silicates, germanates and titanates with ABO_3 stoichiometry,” *Phys. Chem. Minerals*, vol. 4, no. 3, pp. 265–273, 1979.
- [40] J. Ko and C.T. Prewitt, “High-pressure phase transition in MnTiO_3 from ilmenite to LiNbO_3 structure,” *Phys. Chem. Minerals*, vol 15, no. 4, pp. 355–362, 1988.
- [41] N.L. Ross, J. Ko, and C.T. Prewitt, “A new phase transition in MnTiO_3 : LiNbO_3 -perovskite structure,” *Phys. Chem. Miner.*, vol. 16, no. 7, pp. 621–629, 1989.
- [42] Y. Syono, H. Sawamoto, and S. Akimoto, “Disordered ilmenite MnSnO_3 and its magnetic property,” *Solid State Commun.*, vol. 7, no. 9, pp. 713–716, 1969.
- [43] K. Leinenweber, W. Utsumi, Y. Tsuchida, T. Yagi, and K. Kurita, “Unquenchable high-pressure perovskite polymorphs of MnSnO_3 and FeTiO_3 ,” *Phys. Chem. Miner.*, vol. 18, no. 4, pp. 244–250, 1991.
- [44] A. Mehta, K. Leinenweber, A. Navrotsky, and M. Akaogi, “Calorimetric study of high pressure polymorphism in FeTiO_3 : The stability of the perovskite phase,” *Phys. Chem. Miner.*, vol. 21, no. 4, pp. 207–212, 1994.
- [45] K. Leinenweber, J. Linton, A. Navrotsky, Y. fei, and J.B. Parise, “High-pressure perovskites on the join CaTiO_3 - FeTiO_3 ,” *Phys. Chem. Miner.*, vol. 22, no. 4, pp. 251–258, 1995.

- [46] T. Hattori, T. Matsuda, T. Tsuchiya, T. Nagai, and T. Yamanaka, "Clinopyroxene-perovskite phase transition of FeGeO_3 under high pressure and room temperature," *Phys. Chem. Miner.*, vol. 26, no. 3, pp. 212–216, 1999.
- [47] K. Leinenweber, Y. Wang, T. Yagi, and H. Yusa, "An unquenchable perovskite phase of MgGeO_3 and comparison with MgSiO_3 perovskite," *Am. Mineral.*, vol. 79, no. 1–2, pp. 197–199, 1994.
- [48] A.W. Sleight and C.T. Prewitt, "Preparation of CuNbO_3 and CuTaO_3 at high pressure," *Mater. Res. Bull.*, vol. 5, no. 3, pp. 207–211, 1970.
- [49] M. Akaogi, K. Abe, H. Yusa, H. Kojitani, D. Mori, and Y. Inaguma, "High-pressure phase behaviors of ZnTiO_3 : ilmenite-perovskite transition, decomposition of perovskite into constituent oxides, and the perovskite-lithium niobate transition," *Phys. Chem. Miner.*, vol. 42, no. 6, pp. 421–429, 2015.
- [50] A.V. Borhade and Y.R. Baste, "Study of photocatalytic asset of the ZnSnO_3 synthesized by green chemistry," *Arabian Journal of Chemistry*, Online: <http://dx.doi.org/10.1016/j.arabic.2012.10.001>, 2012.
- [51] H. Mizoguchi and P.M. Woodward, "Electronic structure studies of main group oxides possessing edge-sharing octahedra: implications for the design of transparent conducting oxides," *Chemistry of Materials*, vol. 16, no. 25, pp. 5233–5248, 2004.
- [52] B. Kolb and A. Kolpak, "Zinc stannate as a solar cell material," *Bull. Am. Phys. Soc.*, vol. 59, 2014.
- [53] B. Kolb and A. Kolpak, "First-principles design and analysis of an efficient, Pb-free ferroelectric photovoltaic absorber derived from ZnSnO_3 ," *Chem. Mater.*, vol. 27, no. 17, pp. 5899–5906, 2015.
- [54] C. Kons, A. Datta, and P. Mukherjee, "Band-gap tuning in perovskite-type ferroelectric ZnSnO_3 by doping and core shell approach for solar cell applications," *Bull. Am. Phys. Soc.*, vol. 60, no. 1, 2015.
- [55] F. Tran and P. Blaha, "Accurate band gaps of semiconductors and insulators with a semilocal exchange-correlation potential," *Phys. Rev. Lett.*, vol. 102, no. 22, Article ID 226401, 2009.
- [56] A.R. Oganov and C.W. Glass, "Crystal structure prediction using ab initio evolutionary techniques: Principles and applications," *J. Chem. Phys.*, vol. 124, no. 24, Article ID 244704, 2006.

- [57] A.O. Lyakhov, A.R. Oganov, H.T. Stokes, and Q. Zhu, “New developments in evolutionary structure prediction algorithm USPEX,” *Comp. Phys. Commun.*, vol. 184, no. 9, pp. 1172–1182, 2013.
- [58] A.R. Oganov, A.O. Lyakhov, and M. Valle, “How evolutionary crystal structure prediction works—and why,” *Acc. Chem. Res.*, vol. 44, no. 3, pp. 227–237, 2011.
- [59] Y. Wang, J. Lv, L. Zhu, and Y. Ma, “CALYPSO: A method for crystal structure prediction,” *Comp. Phys. Commun.*, vol. 183, no. 10, pp. 2063–2070, 2012.
- [60] G. Kresse and J. Hafner, “Abinitio Molecular-Dynamics for Liquid-Metals,” *Phys. Rev. B*, vol. 47, no. 1, pp. 558–561, 1993.
- [61] G. Kresse and J. Furthmüller, “Efficiency of ab-initio total energy calculations for metals and semiconductors using a plane-wave basis set,” *Computational Mat. Sci.*, vol. 6, no. 1, pp. 15–50, 1996.
- [62] G. Kresse and D. Joubert, “From ultrasoft pseudopotentials to the projector augmented-wave method,” *Phys. Rev. B*, vol. 59, no. 3, pp. 1758–1775, 1999.
- [63] P. Blaha, K. Schwarz, G. Madsen, D. Kvasnicka, and J. Luitz, User’s Guide: “WIEN2K: an augmented plane wave + local orbitals program for calculating crystal properties,” 2001.
- [64] H. Monkhorst and J. Pack, “Special points for Brillouin-zone integrations,” *Phys. Rev. B*, vol. 13, no. 12, pp. 5188–5192, 1976.
- [65] J.A. Brehm, J.W. Bennett, M.R. Schoenberg, I. Grinberg, and A.M. Rappe, “The structural diversity of ABX_3 with d^0 electronic configuration for the B cation,” *J. Chem. Phys.*, vol. 140, no. 22, Article ID 224703, 2014.
- [66] R. Resta, “Macroscopic electric polarization as a geometric quantum phase,” *Europhys. Lett.*, vol. 22, no. 2, pp. 133–138, 1993.
- [67] R.D. King-Smith and D. Vanderbilt, “Theory of polarization of crystalline solids,” *Phys. Rev. B*, vol. 47, no. 3, pp. 1651–1654, 1993.